# Domain Wall Displacement is the Origin of Superior Permittivity and Piezoelectricity in $BaTiO_3$ at Intermediate Grain Sizes

*Dipankar Ghosh, Akito Sakata, Jared Carter, Pam A. Thomas, Hyuksu Han, Juan C. Nino, and Jacob L. Jones**

**The dielectric and piezoelectric properties of ferroelectric polycrystalline materials have long been known to be strong functions of grain size and extrinsic effects such as domain wall motion. In $BaTiO_3$, for example, it has been observed for several decades that the piezoelectric and dielectric properties are maximized at intermediate grain sizes (≈1 μm) and different theoretical models have been introduced to describe the physical origin of this effect. Here, using in situ, high-energy X-ray diffraction during application of electric fields, it is shown that 90° domain wall motion during both strong (above coercive) and weak (below coercive) electric fields is greatest at these intermediate grain sizes, correlating with the enhanced permittivity and piezoelectric properties observed in $BaTiO_3$. This result validates the long-standing theory in attributing the size effects in polycrystalline $BaTiO_3$ to domain wall displacement. It is now empirically established that a doubling or more in the piezoelectric and dielectric properties of polycrystalline ferroelectric materials can be achieved through domain wall displacement effects; such mechanisms are suggested for use in the design of new ferroelectric materials with enhanced properties.**

## 1. Introduction

Size effects in ferroic materials are of fundamental importance and play a crucial role in the functionality of devices at increasingly smaller length scales.[1–5] In polycrystalline ferroelectrics, size effects are chiefly evident in materials properties such as the relative dielectric permittivity ($\varepsilon_r$) and piezoelectric coefficients (e.g., $d_{33}$ and $d_{31}$). For polycrystalline barium titanate ($BaTiO_3$), the effect of grain size on the relative permittivity has been extensively reported over the past decades[3,4,6–20] and is of particular relevance to the continuous size reduction of $BaTiO_3$ capacitors. Within the grain size range of 1–10 μm, it is now widely accepted that $\varepsilon_r$ of polycrystalline $BaTiO_3$ increases with decreasing grain size, reaching a value of 5000, or higher, as the grain size approaches 1 μm. Below 1 μm, however, $\varepsilon_r$ of $BaTiO_3$ decreases markedly with further decreasing grain size. The superior $\varepsilon_r$ values of $BaTiO_3$ at an intermediate grain size of approximately 1 μm exceed those measured in $BaTiO_3$ single crystals ($\varepsilon_{[100]}$ = 4000; $\varepsilon_{[001]}$ = 170)[7] and, furthermore, cannot be explained by orientational averaging of the single crystal anisotropic permittivity values. Limited studies have also shown comparable increases in the piezoelectric coefficients, $d_{33}$ or $d_{31}$, at intermediate grain sizes near 1 μm.[6,21]

Two widely known theories attribute the origin of the superior relative permittivity in polycrystalline $BaTiO_3$ at intermediate grain sizes to either an internal residual stress that changes the domain architecture and increases the intrinsic contribution[5,7,8,22] or enhanced motion of 90° domain walls resulting in increased extrinsic contribution.[9–11,19] A complete and quantitative separation of the effects of internal stress and domain wall dynamics as a function of grain size is yet to be provided. This knowledge gap is primarily attributed to the lack of in situ crystallographic or microstructural investigations during application of applied electric fields. Such in situ studies can uniquely measure the dynamics and mechanics of domains as a function of grain size as well as provide insight into the internal stress states of materials. Here, we undertake such measurements using an in situ high-energy X-ray diffraction (XRD) technique in transmission geometry during application of external electric fields of strong amplitude (above the ferroelectric coercive field, $E_c$) and weak amplitude (below $E_c$). This technique reveals the time-resolved crystallographic changes in $BaTiO_3$ as a function of grain size during electric field application.

Dr. D. Ghosh, A. Sakata, J. Carter, H. Han,
Prof. J. C. Nino, Prof. J. L. Jones
Department of Materials Science and Engineering
University of Florida
Gainesville, FL 32611, USA
E-mail: jacobjones@ncsu.edu
Dr. D. Ghosh
Division of Engineering and Applied Science
California Institute of Technology
Pasadena, CA 91125, USA
Prof. P. A. Thomas
Department of Physics
University of Warwick
Coventry, CV4 7AL, UK
Prof. J. L. Jones
Department of Materials Science and Engineering
North Carolina State University
Raleigh, NC 27695, USA

**DOI: 10.1002/adfm.201301913**

High-energy X-rays are particularly beneficial in the study of ferroelectric polycrystalline materials because they can penetrate entire milimeter-sized samples, meaning the measured diffraction patterns can be said to capture the average behavior of all crystallites in the polycrystalline aggregate, which is a necessary requirement for making quantitative structure-property relationships. In polycrystalline ferroelectrics prior to electric field application, there is no preferred orientation of grains or domains. A preferred domain texture evolves during electric field application as a fraction of the non-180° ferroelectric/ferroelastic domains reorient towards a more preferred direction relative to the applied field.[23] During this domain reorientation, crystallographic and microstructural effects as a result of electric-field-induced lattice strain and domain wall motion can be measured using X-ray and neutron diffraction.[24–31] Domain reorientation, specifically, can be quantified using the intensity interchange between the different orientation variants. Thus, diffraction provides one route to assess the two competing theories described above and will help to understand the structural origin of grain size effects in $BaTiO_3$.

Using this in situ, high-energy XRD technique across the grain size range of 0.2 μm to 3.5 μm, we show conclusive and direct evidence that 90° domain wall motion in $BaTiO_3$ is present during both strong and weak field amplitudes (i.e., corresponding to field amplitudes significantly above and below the macroscopic ferroelectric coercive field). Most importantly, domain wall motion reaches a maximum at a grain size of ≈2 μm where the relative permittivity and piezoelectric coefficient are also maximized. Additionally, measurement of the unit cell volume and spontaneous lattice strain prior to electric field application evidences that the change in residual internal stress across this grain size range is small. We therefore conclusively attribute 90° domain wall motion to the superior properties in $BaTiO_3$ of intermediate grain sizes (≈1–2 μm). Moreover, the in situ measurements reveal, unexpectedly, that application of strong electric field amplitudes triggers an additional reversible phase transition through internal elastic interaction, which is most apparent in the coarse-grained $BaTiO_3$ ferroelectrics.

## 2. Results and Discussion

### 2.1. Permittivity and Piezoelectric Coefficient as a Function of Grain Size

Using both spark plasma sintering (SPS)[32,33] and conventional pressureless sintering, polycrystalline $BaTiO_3$ of six different grain sizes were synthesized. The average grain sizes ranged from ≈0.2 to 3.5 μm (**Figure 1**a), which span the behavioral regimes introduced earlier. The grain size distributions are provided in the supporting information. Annealing was also undertaken on all samples in flowing oxygen in order to mitigate residual stresses and oxygen non-stoichiometry of the samples; this procedure is described in the experimental section and additional information is provided in supporting information. Figure 1b presents both the relative permittivity ($\varepsilon_r$) and the direct longitudinal piezoelectric coefficient ($d_{33}$) of the

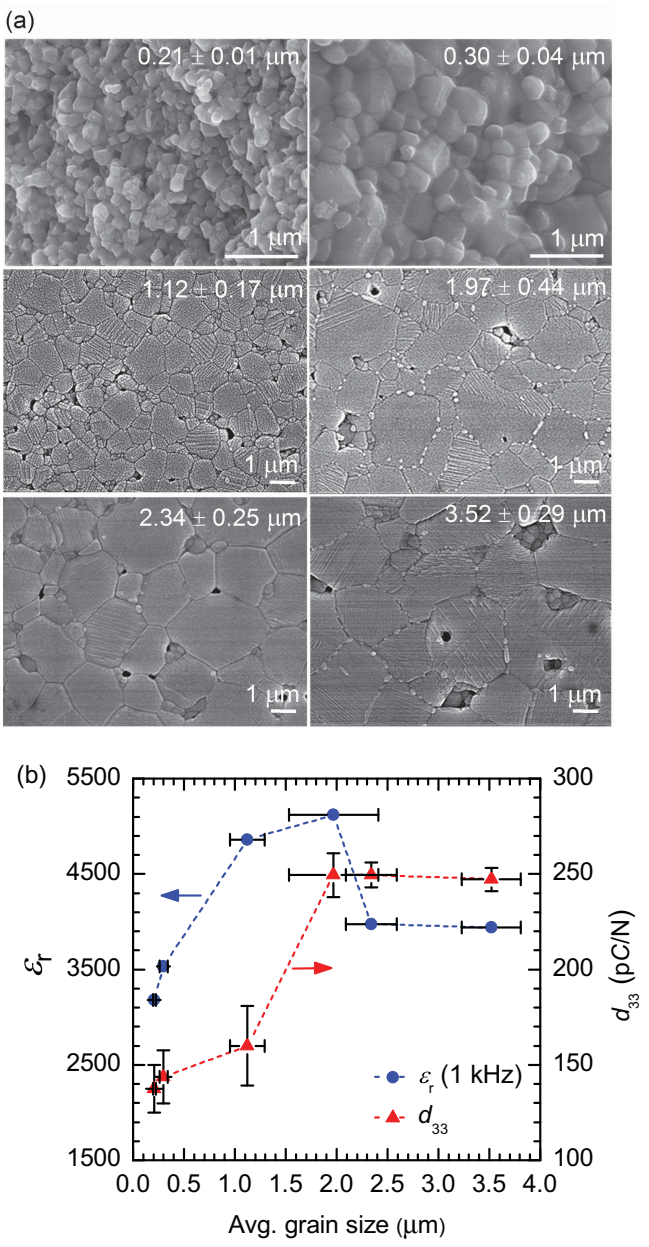


**Figure 1.** a) Microstructures of $BaTiO_3$ of different grain sizes and b) relative permittivity and longitudinal piezoelectric coefficient measurements.

synthesized polycrystalline $BaTiO_3$ samples at room temperature. Within the investigated grain size range, $\varepsilon_r$ is observed to be maximum (>5000) at ≈2 μm and values of $\varepsilon_r$ decrease both above and below this grain size, which agrees with previously reported trends.[3,4,9–11] The permittivity was also measured as a function of temperature up to temperatures exceeding the Curie temperature ($T_c$) and the response at 1 kHz is reported in the supporting information. The $T_c$ remains nearly constant for all grain sizes and the associated loss increases slightly with decreasing grain size as expected. The longitudinal piezoelectric coefficients ($d_{33}$) measured on the same samples reveal a similar trend with room temperature $d_{33}$ reaching a maximum at the grain size of ≈2 μm.

### 2.2. Previous Theoretical Models

Before proceeding, we briefly review the two theories of superior permittivity in ferroelectric $BaTiO_3$ at grain sizes of ≈1–2 μm, specifically the models of residual stress and 90° domain wall contribution. The phenomenological residual stress model attributes the observed peak in $\varepsilon_r$ at approximately 1 μm grain size in polycrystalline $BaTiO_3$ to an increased internal residual stress at this grain size.[5,7,8,22] This internal residual stress is said to arise during the paraelectric cubic to ferroelectric tetragonal phase transition at the Curie temperature[5,7,8,22,34] and is relieved to some extent due to formation of the ferroelectric/ferroelastic tetragonal domains within each single grain of $BaTiO_3$ at room temperature. At grain sizes close to 1 μm, it was originally argued that the 90° domain walls do not form and, therefore, the internal residual stress is not as relieved as the larger grain sizes. This residual stress is then thought to suppress the tetragonality of the $BaTiO_3$ lattice, thus retaining a structure closer in proximity to the cubic state. Since the relative permittivity of $BaTiO_3$ is significantly higher in states nearer the $T_c$ compared to that at room temperature, a sharp increase in $\varepsilon_r$ would be observed at grain sizes close to 1 μm.[5,7,8,22] This argument was largely disputed in Frey and Payne by showing that $T_c$ was nearly constant with grain size for samples synthesized by a sol–gel method.[35]

After the existence of 90° domain walls was later revealed below 1 μm,[9–11] Arlt et al.[9] introduced an alternate model which attributes the superior permittivity in polycrystalline $BaTiO_3$ of intermediate grain size to 90° domain walls. In this model, the permittivity increases from grain sizes of 10 μm down to grain sizes of ≈1 μm due to an increase in 90° domain wall density. Additionally, it was assumed that the contribution of domain walls was due to their displacement or motion during perturbation; it was much later that the intrinsic response of domain walls themselves were clearly observed to enhance property coefficients (e.g., as shown by Wada et al. in $BaTiO_3$ single crystals.[36] In the original model by Arlt et al., it was also assumed that the force constant for 90° domain wall displacement is independent of domain width. Later, Arlt and Pertsev[37,38] calculated a domain width dependence of the force constant that changed between coarse-grained microstructures (banded domain structure wherein each band has a regular laminar structure) and finer-grained microstructures (regular laminar domain structure). According to these calculations, the force constant is higher in fine-grained microstructures than in coarse-grained microstructures. As a result, domain walls in thinner domain structures are more difficult to move than domain walls in thicker domain structures. Due to the stiffer force constant predicted in $BaTiO_3$ of smaller grain size, Arlt and Pertsev[37] suggested that the higher permittivity at grain sizes near 1 μm may not be caused by the high density of 90° domain walls as was suggested earlier.[9] However, it was also rationalized that as the grain size decreases towards 1 μm, a strong softening of the force constant may be expected owing to the reduction of stresses in and near the grain boundary areas. This, in turn, may act as a feedback and ultimately enhance the domain wall contribution in grain sizes of ≈1 μm.[37]

Below a grain size of ≈1 μm, the decrease in permittivity is considered to arise from both the lowering of 90° domain wall density and restricted domain wall motion. These effects thus reduce the contribution of 90° domain walls to relative permittivity. Damjanovic[39] supported these observations by showing that activity of domain walls becomes weaker in $BaTiO_3$ of finer grain size (0.7 μm) than in $BaTiO_3$ of coarser grain size (26 μm) because the domain walls are relatively more clamped in the former than in the latter. For even smaller grain sizes below 300–500 nm, the grain size starts to become comparable to the size of a single domain. As a result, the domain wall displacement and nucleation of new domains become more difficult under application of electric fields or stress.[3,4] Direct experimental measures of the grain size dependence of domain wall motion and its contribution to macroscopic property coefficients is needed in order to reconcile these various effects, in particular in a range of grain sizes that transcend the 1–2 μm grain size range of enhanced property coefficients (e.g., Figure 1b).

### 2.3. Structural Changes and Residual Stress as a Function of Grain Size

High-energy XRD patterns of the {200} and (111) Bragg reflections measured prior to electric field application are shown in **Figures 2**a,b, respectively. These diffraction patterns indicate some systematic structural changes with grain size. Figure 2a shows extremely weak splitting of the (002) and (200) Bragg reflections in the smallest grain size (≈0.2 μm) and the extent of splitting increases with increasing grain size. The (200) peak positions (related to the *a* lattice parameter) remain almost constant with increasing grain size whereas the (002) peak position (related to the *c* lattice parameter) shifts consistently to higher lattice spacing (lower $2\theta$) as the grain size increases. Additionally, increased diffuse scattering or additional X-ray intensity between the (002) and (200) Bragg reflections is observed with decreasing grain size. This increase in the diffuse scattering may suggest either that the density of domain walls increases with grain size reduction (e.g., as reviewed elsewhere)[40] and/or that the strain field surrounding the 90° domain walls increases in the smaller grain sizes.[10,41,42] As the density of domain walls is clearly a defining variable to property coefficients in single crystal $BaTiO_3$,[36] it is tempting to speculate that an increase in domain wall density (as may be indicated in the present work by the increased diffuse scattering) may lead to increased property coefficients. However, the dielectric and piezoelectric coefficients do not correlate proportionally to the diffuse scattering, instead maximizing at ≈2 μm. Thus, the domain wall density in and of itself is insufficient to explain the observed superior properties at ≈2 μm. Finally, Figure 2b shows some systematic changes in the (111) Bragg reflection with grain size variation, though the differences are less pronounced than in the {200} reflections. In the grain sizes of ≈0.2 and 0.3 μm, the peak broadening of the (111) reflection relative to the larger grain sizes is most pronounced.

To quantify the structural changes in $BaTiO_3$ as a function of grain size, lattice parameters (*c* and *a*), lattice aspect ratio ($c/a$), unit cell volume, and full width at half maximum (FWHM) were further evaluated. The lattice parameters were determined from the (002) and (200) Bragg reflections, and subsequently used to calculate the $c/a$ and unit cell volume ($a \times a \times c$). The (002) and (200) Bragg reflections were fitted

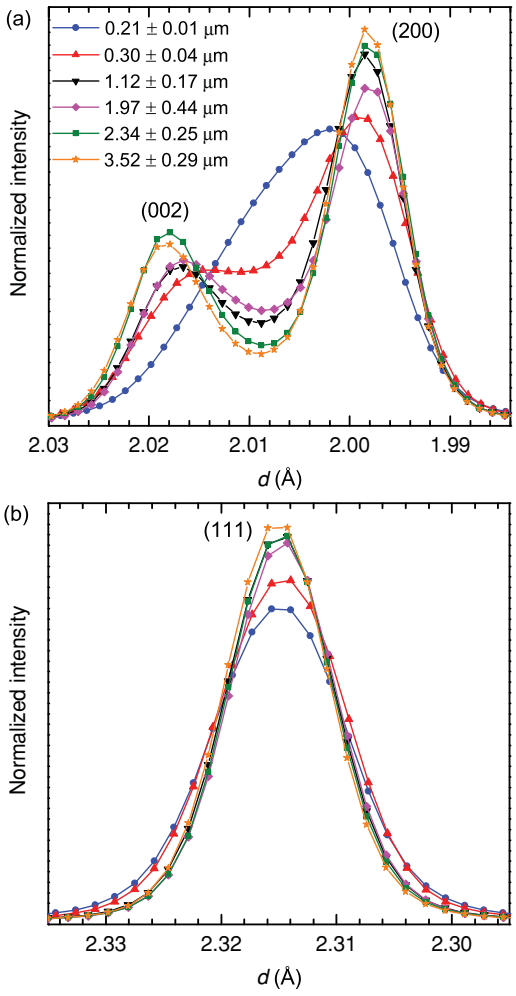


**Figure 2.** High-energy X-ray patterns of a) {200} and b) (111) Bragg reflections prior to electric field application.

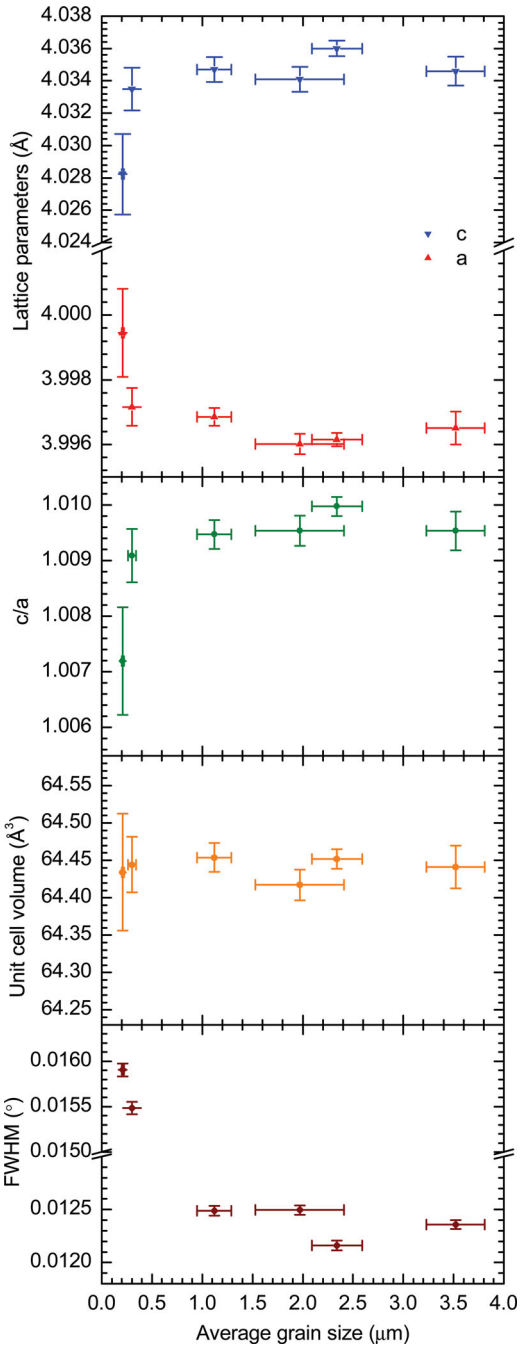


**Figure 3.** Variation in a) tetragonal lattice parameters (*c* and *a*), b) *c*/*a*, c) unit cell volume, and d) FWHM of (111) Bragg reflection as a function of average grain size of the synthesized $BaTiO_3$ samples.

with the pseudo-Voigt profile shape function and the lattice parameters were determined from the central peak positions of the fitted profiles.[42] FWHM values reported here were determined from the (111) reflections because of their reduced sensitivity to diffuse scattering from domain walls relative to the {002} Bragg reflections. The FWHM values were determined by fitting the profile to a Pearson VII-type profile shape function. These respective profile shape functions were empirically found to best describe the respective measured diffraction profiles. Examples of fitted profiles are shown in supporting information.

**Figure 3**a shows the changes in lattice parameters with grain size. Using these lattice parameters, the *c*/*a* and unit cell volumes (Figures 3b,c, respectively) are useful in assessing the dependence of spontaneous ferroelastic strain and residual stress on grain size. The decrease in the *c*/*a* (Figure 3b) with decreasing grain size indicates that $BaTiO_3$ becomes less tetragonal at smaller grain sizes, which is consistent with earlier reports.[3,9,43,44] Notably, however, the asymmetric {200} diffraction profile of the smallest grain size material (≈0.2 μm) shows that the tetragonal phase is still retained. In contrast, the unit cell volume (Figure 3c) remains almost constant across the entire grain size range of ≈0.2 to 3.5 μm.

Figure 3d shows the FWHM values of the (111) Bragg reflection as a function of grain size. Among all the grain sizes, the largest FWHM is observed at the smallest grain size of ≈0.2 μm and decreases with increasing grain size though the changes become less significant in the largest grain sizes. The observed

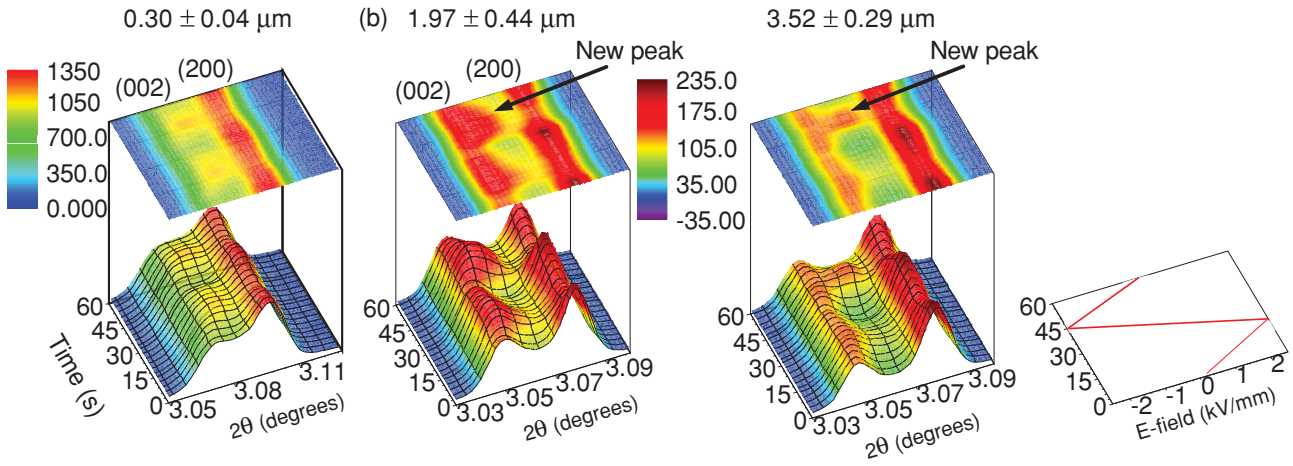


**Figure 4.** Contour plots of changes in intensities of (002) and (200) reflections during high electric field application (±2.5 kV mm$^{-1}$) revealing variation in 90° domain wall motion for a) 0.3 μm), b) ≈2 μm, and c) ≈3.5 μm grain sizes of $BaTiO_3$.

broadening of the (111) Bragg reflection at grain sizes of ≈0.2 and 0.3 μm can be attributed to either a crystallite size effect and/or increased microstrain relative to $BaTiO_3$ of larger grain sizes. Microstrain is described with a change in the distribution of lattice spacings; in contrast, a change in the average lattice plane position, or macrostrain, would be observed as shifts in the Bragg peak(s) and would be a measure of residual stress. The (111) peak positions are nearly independent of grain size, indicating that the macrostrain remains almost constant over the entire grain size range of ≈0.2–3.5 μm. This observation from the (111) Bragg peaks is consistent with the observation from the {002} Bragg peaks that the unit cell volume (Figure 3c) remains approximately constant.

As discussed before, the phenomenological residual stress theory attributes the presence of a large residual stress to the sharp increase in the relative permittivity of $BaTiO_3$ in grain sizes of approximately 1–2 μm. Since the $\varepsilon_r$ is observed to be maximum at ≈2 μm in the present work (Figure 1), the phenomenological residual stress theory would suggest that residual stress should be maximum at this grain size. Observations presented thus far from XRD patterns obtained prior to electric field application (Figures 2b, 3d), however, do not show a significant variation in residual stress across the grain size range of 1–3.5 μm. In contrast, the X-ray measurements may indicate a higher level of microstrain at grain sizes of ≈0.2 and 0.3 μm, though these grain sizes exhibit lower relative permittivity and piezoelectric coefficients. Therefore, the observed increase in the relative permittivity and piezoelectric coefficient at the grain size of ≈2 μm cannot be reconciled by the residual stress theory.

### 2.4. In Situ X-ray Diffraction During Strong Electric Field Application

In order to measure the electric field-induced structural changes in polycrystalline $BaTiO_3$, high-energy XRD measurements were undertaken on samples across the grain size range of ≈0.2–3.5 μm. Since the high-energy X-rays can penetrate a large volume of material, high-energy XRD effectively measures the collective effect of the microscopic displacements of domain walls. These measurements are therefore utilized to interpret the effect of domain wall motion on the macroscopic property coefficients.[26,30,45]

#### *2.4.1. 90° Domain Wall Motion During Strong Electric Field Application*

The structural response of ferroelectric $BaTiO_3$ to strong electric field amplitudes, or amplitudes exceeding $E_c$, is first presented. XRD patterns near the {200} diffraction profile are used to show the extent of domain wall motion during a bipolar electric field (±2.5 kV mm$^{-1}$) of triangular waveform. These results are shown in **Figure 4** for three different grain sizes of 0.3, ≈2, and ≈3.5 μm which represent typical behaviors measured in the grain size regimes below 1 μm (Figure 4a), near 1–2 μm (Figure 4b), and above 2 μm (Figure 4c), respectively. Additional measurements for other grain sizes are provided in the supporting information. It can be seen in Figure 4 that all of the measured grain sizes exhibit an exchange of intensity in the (002) and (200) Bragg reflections during electric field application. It is important to note that intensity interchange in these reflections of perovskite ferroelectrics has been shown to be indicative of 90° domain reorientation.[26,30] The present measurements therefore reveal direct evidence of 90° ferroelectric/ferroelastic domain wall motion during electric fields of high amplitude in polycrystalline $BaTiO_3$ for all the grain sizes investigated.

Representative X-ray line patterns measured at several specific states of the electric field waveform are further shown in the supporting information and highlight the quantitative changes in the diffraction patterns as a function of grain size and electric field amplitude and history. For the 0.3 μm grain size (Figure 4a), the XRD data indicates that the intensities of the (002) and (200) reflections increase and decrease, respectively, with increasing field magnitude during both polarities of

the field. It is also observed that the (200) peak position remains almost unchanged during the electric field application while the (002) peak position shifts to higher $2\theta$ (or lower $d$) with increasing electric field during both the positive and negative waveforms. For the ≈2 μm grain size (Figure 4b), a dramatic change in the (002) and (200) peak intensities during electric field application is observed, which indicates a significantly enhanced 90° domain wall motion relative to that observed at the grain size of 0.3 μm. At a grain size of ≈3.5 μm (Figure 4c), significant 90° domain wall motion is also observed, though to a lesser extent than at a grain size of ≈2 μm.

Summarizing these observations from Figure 4, it is clear that significant 90° domain wall motion occurs during the bipolar high-field cycling at grain sizes of ≈2 and ≈3.5 μm whereas less 90° domain wall motion occurs at the smaller grain size of 0.3 μm. Thus, 90° domain wall motion is seen to increase with increasing grain size from 0.3 to ≈2 μm, then decrease slightly with a further increase in the grain size to ≈3.5 μm. These trends are consistent with the trends in $\varepsilon_r$ and $d_{33}$ introduced previously in Figure 1b. The in situ X-ray measurements thus provide direct evidence of the grain size dependence of 90° domain wall motion which correlates with the increased property coefficients measured at ≈2 μm. The observed results therefore support the theory attributing higher 90° domain wall contribution to the superior permittivity and piezoelectricity in $BaTiO_3$ at intermediate grain sizes.

#### 2.4.2. Field-Induced Phase Transition in $BaTiO_3$

The in situ X-ray measurements show an additional interesting structural feature during application of the highest electric field amplitudes in certain grain sizes (≈2 and ≈3.5 μm), an additional Bragg reflection appears in between the (002) and (200) tetragonal phase reflections. These measurements indicate a field-driven polymorphic phase transition in $BaTiO_3$ during strong electric field amplitude. It is interesting to note that the observed phase transition becomes prominent near the maximum of the field amplitude (2.5 kV $mm^{-1}$) and subsequently disappears at zero field. The in situ X-ray measurements enable the observation of both the phase transition and its reversibility.

In order to further characterize the field-induced polymorphic state, the {200} composite diffraction profile is fit with three symmetric profile functions. Examples of resultant fits are shown in the supporting information. It can be seen that all the three Bragg reflections can be fit with three symmetric pseudo-Voigt profiles. This result could imply that the additional peak in the middle of this diffraction profile is a single reflection, although any additional subtle peak splitting may not be resolved within the available instrumental resolution. The field-induced peak in the middle of the {002} diffraction profile is therefore interpreted as a different polymorphic phase of unknown symmetry.

Field-induced phase transitions in $BaTiO_3$ have been reported previously,[46–50] and some of these studies[46–48] showed that the Curie temperature is shifted to higher values in the presence of an electric field, suggesting the proximity to a cubic phase decreases, or equally that the proximity to the orthorhombic phase increases. It is therefore possible that the field-induced phase is of orthorhombic symmetry. Further, other studies on $BaTiO_3$ single crystals[49,50] have reported an electric field-induced monoclinic phase close to the tetragonal-orthorhombic phase transition temperature. Once formed, this monoclinic phase is observed to be stable even upon removal of the field, a characteristic that is not observed in the present field-induced transition, though does not eliminate this phase from being the phase observed in the present work. It is also possible that the induced phase may be nonpolar (e.g., cubic) if the driving force is related to intergranular or other mechanical interactions within the grains.

Although the instrument resolution in the present work is not suitable for assigning a specific symmetry to this field-induced phase, some characteristics of this field-induced phase are worth noting in the present work. Though observed under both positive and negative polarity, the intensity of this new phase is consistently stronger under negative field amplitudes. Since this phase transition is observed at grain sizes in which the 90° domain wall motion is the greatest, it is considered that the structural origin of this phase transition is associated with the large strain of the polycrystalline aggregate and the extensive 90° domain wall motion in these grain sizes. The proposed structural origin is now discussed in more detail using the ≈3.5 μm grain size $BaTiO_3$ as a representative example (Figure 4c, with specific profiles shown in the Supporting Information, Figure S6f). At the maximum of positive and negative polarities, the (002) intensity is nearly constant, implying that the volume fraction of *c*-axis-oriented domains does not change significantly between the polarities. In contrast, a significant decrease in the (200) intensity is observed during the negative polarity relative to that during the positive polarity. This indicates that there is a further decrease in the volume fraction of the *a*-axis-oriented domains during the maximum of negative polarity relative to that during the maximum of positive polarity. This is unlike the typical (002) and (200) intensity interchange that is observed during domain reorientation of single phase tetragonal perovskites.[23,26] The observations for negative electric field polarity indicates that a fraction of the *a*-axis-oriented domains of the tetragonal phase change transform into the field-induced structure which exhibits the intermediate {002} diffraction peak.

A simplified schematic of this proposed mechanism is presented in **Figure 5**, which illustrates a simplified 90° domain configuration and the electromechanical strain interaction mechanism. In the initial state prior application of any electrical field (Figure 5a), the black rectangles represent domain orientation states within a single representative grain that are separated by 90° domain walls. During application of the electric field, strain is known to occur in ferroelectrics through 90° ferroelectric/ferroelastic domain wall motion and electric-field-induced distortion of the individual domains (e.g., piezoelectric strain). Within a single grain, these two mechanisms interplay and ultimately achieve an equilibrium response. It is further understood that domain wall motion within polycrystalline materials never results in a complete c-axis-oriented domain state due to intergranular mechanical constraints; remanent *a*-axis oriented domains remain in nearly all materials. These remanent *a*-axis oriented domains are observed in the present experiments in the (200) intensity of the tetragonal phase. If the energy barrier for transition into an alternate polymorphic phase is low

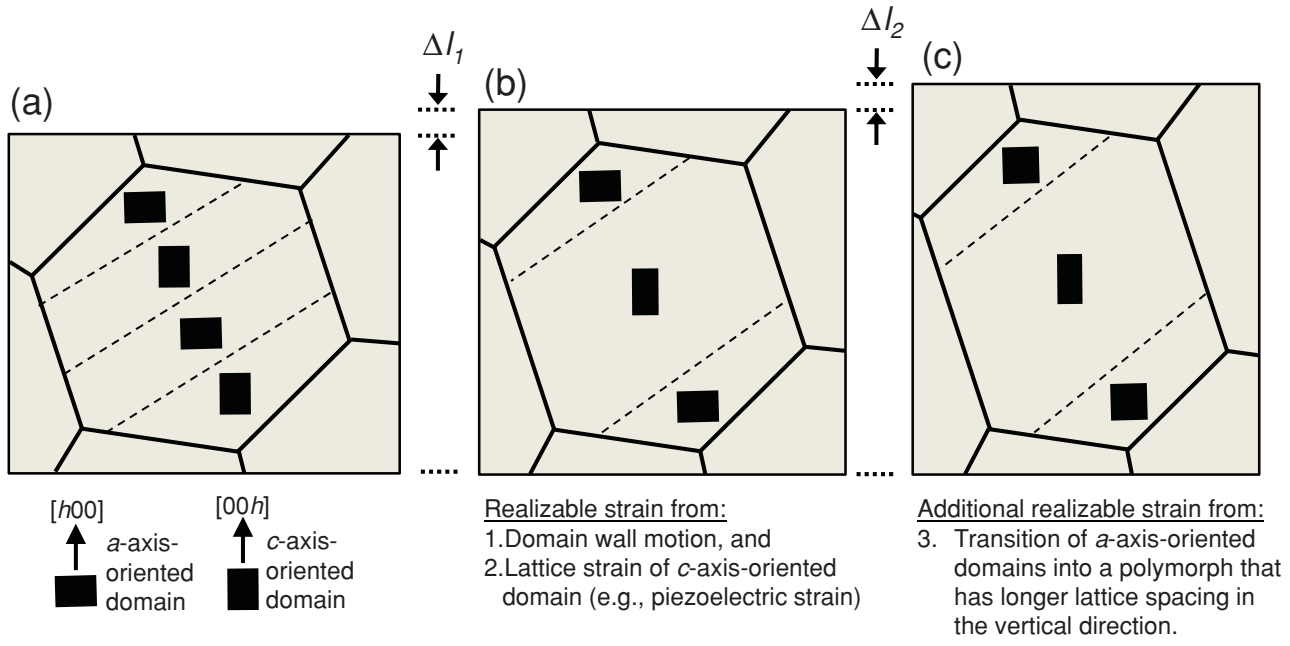


**Figure 5.** Simplified illustration of an electromechanical strain mechanism in which a-axis oriented domains transform into a new polymorph in order to facilitate strain of a crystalline grain. a) In the initial state, the black rectangles represent domain orientation states within a single representative grain that are separated by domain walls. b) Strain is achieved through domain wall motion and distortion of the unit cells (e.g., piezoelectric strain). c) Additional strain is enabled from the phase transition mechanism.

(e.g., due to the residual or induced stress state in polycrystals, proximity to the phase transition in temperature or composition, etc.), then it will be more favorable for the remanent *a*-axis-oriented domains to transform into this new ferroelastic strain state than for *c*-axis oriented domains. If *a*-axis-oriented domains transform into this new polymorph, then the strain of the transformed material will more closely parallel the effective strain of the crystal and polycrystalline aggregate.

The diffraction patterns for the other samples with grain sizes >1 μm also show evidence that this field-induced, reversible phase transition may be present, though is not observed as clearly as in the sample with 3.5 μm grain size. The differences between different grain sizes may be a result of the crystal or domain sizes (which may affect the ability to observe the effect in diffraction), or there may exist a change in the expression of this effect in smaller grain sizes. Nevertheless, it is clear in the current in situ X-ray measurements that a reversible, field-induced phase transition is triggered during electric field amplitudes greater than the ferroelectric coercive field in coarse grained $BaTiO_3$ at room temperature.

### *2.4.3. Determination of the Extent of 90° Domain Reorientation*

Using diffraction, 90° domain wall motion in single-phase tetragonal ferroelectrics is traditionally quantified from changes in the volume fractions of the (002) and (200) orientation variants during electric field application. In the present work, a clear separation of the (002) and (200) diffraction intensities is not possible due to the presence of the field-induced polymorph at strong electric field amplitudes. We therefore introduce here a new method to associate changes in the {002} diffraction profile with the macroscopic strain of the sample. The method uses the cumulative diffraction intensity distribution of interplanar spacing, *d*, across the {002} diffraction profile. The change in the median of this distribution can be used as a measure of the change in the type, proportions, and strain of {002} planes of a particular orientation in the sample. Thus, it is a measure of the combined effect of {002} lattice strains, 90° domain volume fractions (domain texture), and changes in phase fractions of coexisting polymorphs. For each cumulative intensity distribution, the median ($d_{50}$) is described by saying that ≈50% of the material in the direction of the electric field has interplanar spacings above $d_{50}$ and ≈50% below $d_{50}$. Differences in structure factors of the tetragonal (002) and (200), and the {002} reflections of the induced polymorph may cause $d_{50}$ to vary from a precise 50% indicator of volume fractions. Nevertheless, it is a useful quantitative metric for evaluating diffraction spectra with multiple overlapping peaks from multiple polymorphs.

**Figure 6**a–c shows XRD patterns measured prior to electric field application, at the maximum field amplitude (both positive and negative polarity), and the corresponding cumulative diffraction intensity distributions of interplanar spacing, *d*, for representative grain sizes 0.3, ≈2 and, ≈3.5 μm. Figure 6d shows resulting changes in the $d_{50}$ values before and during electric field application for these grain sizes. Several observations can be made from Figure 6d. For all the grain sizes, the $d_{50}$ values are higher during electric field application than prior to field application. This correlates with a positive electric-field-induced strain in {002}-oriented crystallites. Additionally, for each grain size, the $d_{50}$ value during negative polarity is observed to be higher than that during positive polarity. The origin of this

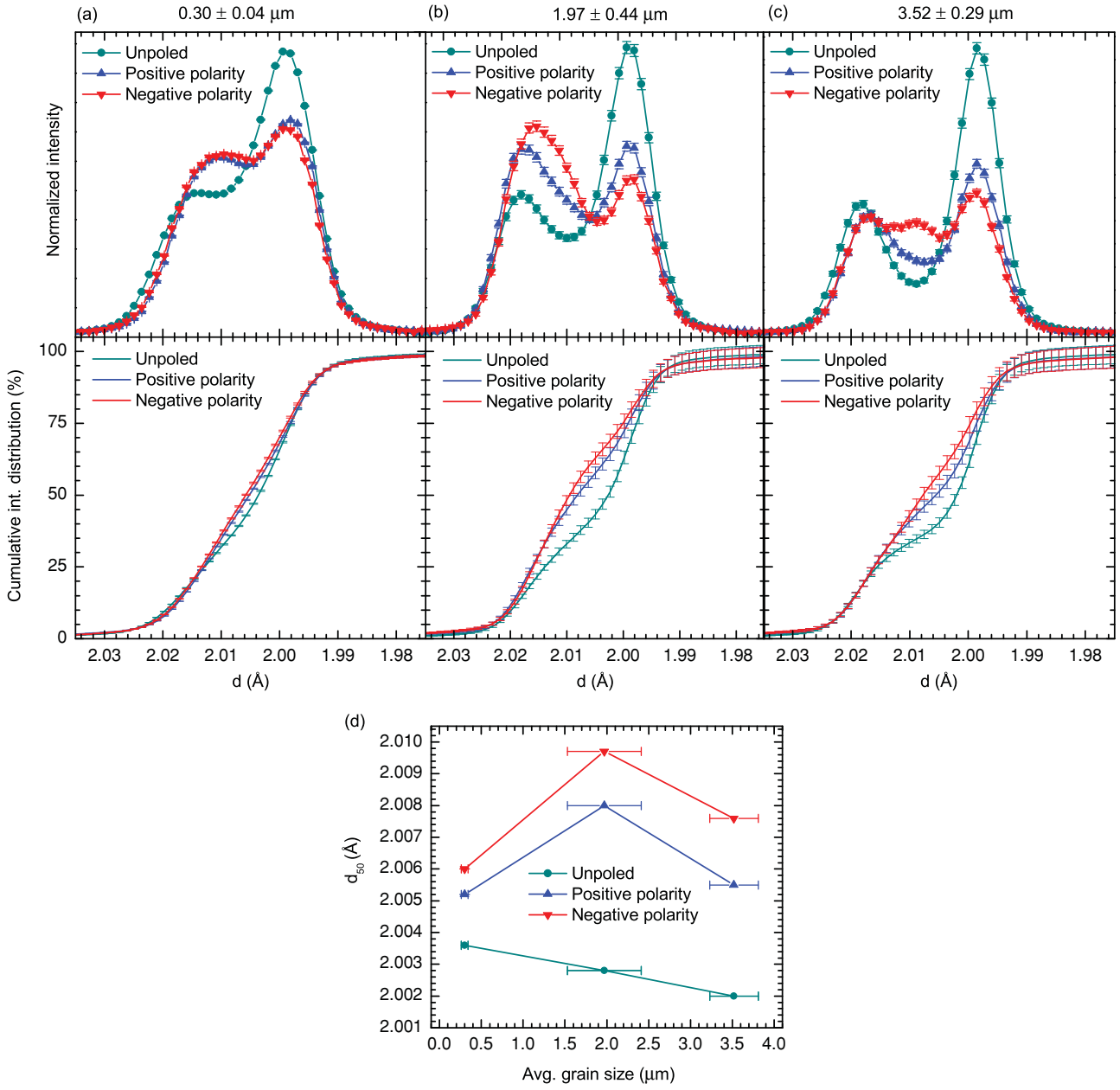


**Figure 6.** Cumulative diffraction intensity distribution of interplanar spacing, *d*, across the {002} diffraction profile for a) 0.3 μm, b) ≈2 μm, and c) ≈3.5 μm grain sizes of $BaTiO_3$ prior to and during application of strong electric field amplitudes (both the positive and negative polarities). d) Calculated $d_{50}$ values as a function of grain size.

asymmetry is unknown, though asymmetries in strain behavior are often observed in ferroelectrics due to extrinsic effects.[45] Most importantly, Figure 6d indicates that change in $d_{50}$ due to the electric field application is maximum at the grain size of ≈2 μm. This means that the combined effect of {002} lattice strains, 90° domain volume fractions (domain texture), and changes in phase fractions of coexisting polymorphs (tetragonal and the field-induced state) is observed to be maximum at the grain size of ≈2 μm. Qualitatively, the observation of the {002} diffraction profiles (e.g., those in Figures S5,S6, Supporting Information) indicate that the dominant contribution to this behavior is from domain wall motion in the tetragonal phase which is observed in intensity interchanges between the tetragonal (002) and (200) reflections. Most notably, this grain size also exhibits the highest relative permittivity and piezoelectric coefficients as previously introduced in Figure 1b.

### 2.5. In Situ X-ray Diffraction During Weak Electric Field Application

Having shown the structural response during strong electric fields, the structural response at weak electric field amplitudes

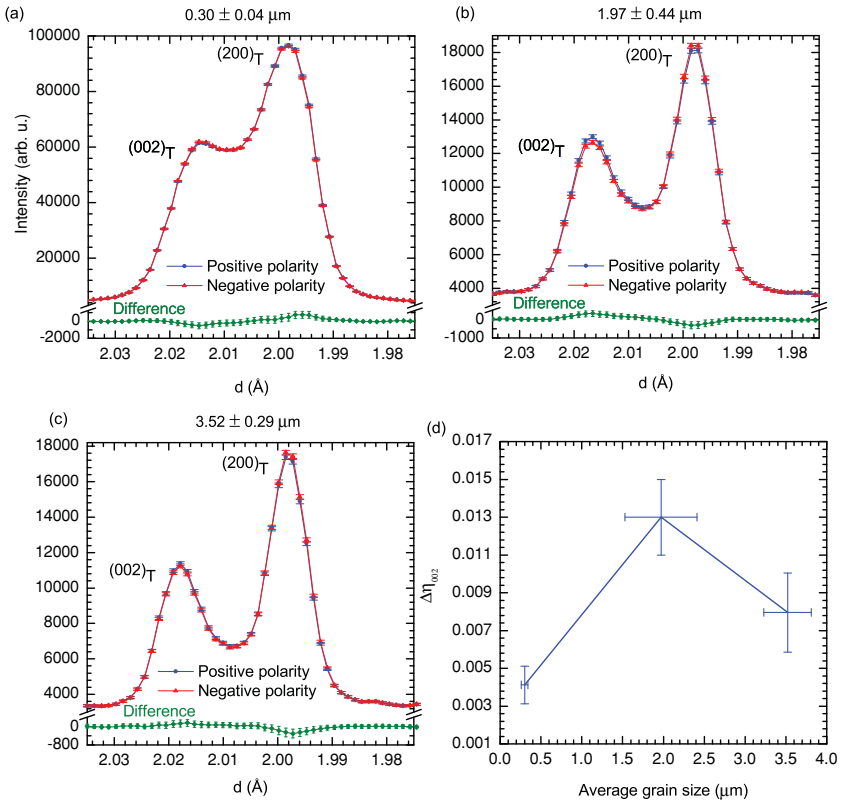


**Figure 7.** XRD profiles of (002) and (200) Bragg reflections during application of weak (subcoercive) electric field amplitudes (±0.2 kV mm$^{-1}$) revealing variation in 90° domain wall motion for a) 0.30 μm, b) 1.97, and c) 3.52 μm grain sizes of $BaTiO_3$. d) Calculated values of domain switching as a function of grain size.

is next examined. While application of electric fields above $E_c$ results in large-scale domain wall motion (and, in certain grain sizes, a field-induced phase transition), small displacements of non-180° domain walls over local energy barriers at subcoercive field amplitudes (those below $E_c$) can be also measured using these X-ray approaches.[30,45,51,52] Such measurements provide a direct assessment of domain wall vibration (reversible) and small irreversible domain wall displacements at weak electric field strengths. Diffraction measurements at such weak fields can reveal the extrinsic contribution of domain wall motion to the property coefficients at conditions comparable to those used in the determination of macroscopic properties including relative permittivity and the piezoelectric coefficients.[27,45,51,52] Direct measurement of domain wall motion at weak field amplitudes can thereby provide further insight into the grain size dependence of 90° domain wall displacements and its relation to the relative permittivity and piezoelectric coefficient of $BaTiO_3$.

**Figure 7**a–c shows representative XRD profiles of 0.3, ≈2, and ≈3.5 μm grain sizes, measured using a square wave bipolar electric field of amplitude 0.2 kV mm$^{-1}$ amplitude (approximately 40% of $E_c$). For each grain size, a subtle difference between the diffraction patterns measured at positive and negative polarities can be observed outside the error bars. This measurement of a very weak effect is made possible through the high intensities achievable at the synchrotron source. These results qualitatively indicate the presence of the 90° domain wall motion at very weak electric field strengths and are consistent with observations of similar effects in lead zirconate titanate (PZT) ceramics.[53] Notably, the intensity differences, and thus domain wall motion, is greatest for the ≈2 μm grain size. In order to quantify domain wall motion due to electric field application, the measured diffraction profiles are fit to pseudo-Voigt shape functions to extract the integrated intensities of (002) and (200) peaks of the tetragonal $BaTiO_3$ phase. Even though the field-induced secondary polymorph is not observed during application of weak electric fields, a third peak is nevertheless required in order to adequately fit the {002} diffraction profiles measured at weak fields because diffuse scattering from 90° domain walls is observed between the tetragonal (002) and (200) reflections.[42] Figure 7d shows the calculated change in volume fraction of the two domain variants between the positive and negative polarities ($\Delta\eta_{002}$) as a function of grain size. This reveals an increase of the $\Delta\eta_{002}$ from the 0.3 μm grain size to the ≈2 μm grain size followed by a continuing decrease in larger in grain sizes. The grain size dependence of 90° domain wall motion observed at weak field amplitude (Figure 7d) is consistent with the observations made at higher field amplitudes (Figure 6). That is, the in situ XRD measurements during both strong and weak electric field application show more domain wall displacement in the grain sizes in which the relative permittivity and piezoelectric coefficients are maximized.

### 2.6. Combined Discussion

In polycrystalline ferroelectrics, the non-lattice extrinsic contribution to the macroscopic property coefficients (e.g., dielectric, piezoelectric and elastic) originates primarily from the collective motion of domain walls and other interfaces. Domain wall motion even at the weak to moderate fields (comparable to conditions where macroscopic property coefficients are measured) leads to the significant extrinsic contributions to the dielectric, elastic, and piezoelectric property coefficients.[30,31,54–59] In many cases, this contribution may be comparable or greater than the intrinsic effect of the lattice itself.[30,60,61] The present work directly reveals that the motion of domain walls in $BaTiO_3$ is greatest at the intermediate grain sizes of ≈2 μm, correlating with the maximum values of permittivity and piezoelectric coefficient. Quantitative evidence of this correlation exists from measurement of the response of the sample under both strong ($d_{50}$) and weak ($\Delta\eta_{002}$) field amplitudes.

With the insight obtained from the in situ XRD measurements, we return to the theories presented earlier that describe the origins of enhanced permittivity and piezoelectric

coefficients at intermediate grain sizes on the order of ≈1 μm. The phenomenological residual stress theory attributed the observed peak in $\varepsilon_r$ at ≈1 μm grain size to an increased internal residual stress.[5,7,8,22] However, the XRD measurements reveal no significant change in residual stress associated with macrostrain as a function of grain size. Thus, while residual stress may have a small effect, we do not observe it to be a dominant factor in the enhancement of relative permittivity and piezoelectric coefficients. The theory introduced by Arlt et al.[9,37,38] attributed the superior permittivity at intermediate grain sizes to the displacement of 90° domain walls in the tetragonal phase. The present in situ XRD measurements confirm the validity of this theory under both strong and weak electric field amplitudes, that is, that an enhanced displacement of 90° domain walls in grain sizes of ≈1–2 μm leads to the enhanced relative permittivity and piezoelectric coefficients in $BaTiO_3$. Moreover, the observation of a reversible, field-induced polymorph in coarse-grained $BaTiO_3$ provides additional insight into the complexity of the micromechanics of polycrystalline ferroelectrics.

We previously showed that the piezoelectric coefficients in La-modified tetragonal PZT approaching the morphotropic phase boundary are dominantly (>50%) derived from the displacement of 90° domain walls.[30] The present work demonstrates both enhanced piezoelectric and dielectric properties in $BaTiO_3$ due to the displacement of domain walls. Holistically, the results of these experiments suggest that the displacement of domain walls and other extrinsic effects dominate the electromechanical response of real ferroelectric materials. Thus, the search for superior dielectric and piezoelectric properties of oxides should consider extrinsic effects as a source for enhanced response. In particular, the present search for superior piezoelectric coefficients in novel (both lead-containing and lead-free) perovskite compounds and solid solutions should consider the effect of domain wall motion to the realizable properties and material behavior. The present work demonstrated the ability to tune this enhanced response using grain size, though additional factors are known to affect domain wall mobility, notably through compositional modification such as donor doping. Theoretical models, including the ones introduced by Arlt et al.,[9,37,38] may be further considered in exploiting these behaviors and properties in real materials.

## 3. Conclusions

In the current work, polycrystalline $BaTiO_3$ ceramics in the grain size range of ≈0.2–3.5 μm were synthesized using conventional pressureless sintering and spark plasma sintering. Relative permittivity and longitudinal piezoelectric coefficient measurements showed that both the coefficients are maximum at approximately ≈2 μm grain size. High-energy X-ray measurements prior to electric field application showed significant structural changes as a function of grain size in $BaTiO_3$, though did not indicate any significant variation of internal residual stress that can be attributed to the observed grain size effects. To study the effect of grain size on domain wall motion, samples were irradiated using high-energy X-rays during application of both strong and weak electric fields. These measurements revealed a strong dependence of grain size on domain wall motion which was observed to be maximum at approximately ≈2 μm, the grain size in which the macroscopic property coefficients also maximize. Based on these results, we validate the theory of Arlt et al.[9,37,38] in attributing the enhanced properties of $BaTiO_3$ to the displacement of domain walls. This knowledge should be used in the design of new materials with superior property coefficients and functionalities.

## 4. Experimental Section

*Material Synthesis, Density Measurements, and Microstructure*: In the current work, $BaTiO_3$ ceramics of six different grain sizes across the grain size range of ≈0.2–3.5 μm were synthesized using spark plasma sintering (SPS) and conventional pressureless sintering of a commercially available nanocrystalline $BaTiO_3$ powder (Alfa Aesar, Ward Hill, MA) of approximate particle size of 50 nm (Figure S1, Supporting Information). Using SPS, $BaTiO_3$ ceramics of 0.21 μm and 0.3 μm grain sizes were synthesized. Other grain sizes (1.12 μm, 1.97 μm, 2.34 μm, and 3.52 μm) of $BaTiO_3$ were synthesized using conventional pressureless sintering. Details of the synthesis of these materials and all the sintering conditions are provided in the supporting information. Densities of the sintered materials were measured using Archimedes technique and the measured density values are listed in Table S1 in supporting information. Average grain sizes of the sintered $BaTiO_3$ ceramics were estimated using lineal intercept technique in accordance with ASTM E112-10 standard test methods for determining average grain size and the grain size values are given in Table S2, Supporting Information. Grain size distributions of all the $BaTiO_3$ ceramics are shown in Figure S2, Supporting Information. Details of the sample preparation for the grain size measurements are also given in the supporting section. Microstructural analyses of the starting powder particles and sintered materials were performed using a field-emission scanning electron microscope (SEM, JEOL 6335F FEG-SEM).

*Relative Permittivity and Piezoelectric Measurements*: The relative permittivity ($\varepsilon_r$) and longitudinal piezoelectric coefficient ($d_{33}$) measurements were conducted on $BaTiO_3$ samples after annealing in air. $\varepsilon_r$ values of the $BaTiO_3$ were measured from room temperature to 200°C using an Agilent 4284A LCR meter in the frequency range of 1 kHz to 1 MHz in a temperature chamber and controller from Delta Design, Inc. For $d_{33}$ measurements, the electroded specimens were placed in a silicone oil bath, poled under a DC field of 2.5 KV $mm^{-1}$ at room temperature for 5 min and $d_{33}$ values were measured using a $d_{33}$ meter (YE2730A, APC Int. Ltd.). Procedures for specimen preparations for the $\varepsilon_r$ and $d_{33}$ measurements are given in the supporting information. All measured values are given in Table S2, Supporting Information.

*High-Energy In Situ XRD During Strong and Weak Electric Field Application*: To explore the grain size dependence of domain wall motion in $BaTiO_3$ ceramics and relation to bulk physical property coefficients, in situ high-energy XRD measurements during electric field application and in transmission geometry were conducted on the 11-ID-C beamline in the Advanced Photon Source (APS) at the Argonne National Laboratory. The high-energy XRD technique is capable of measuring the collective and average response of a large volume of the sample. In situ high-energy XRD during external electric fields enables investigation of crystallographic and microstructural changes in real time and macroscopic domain wall displacements can be quantified during the conditions at which properties and electromechanical behavior are characterized. The high energy of the X-ray beam (≈110 keV) is highly penetrating and a wide coverage of reciprocal space is measured over a small angular scattering range. For each grain size $BaTiO_3$ sample, high-energy XRD patterns were measured initially on unpoled samples. Next, samples were electrically poled under bipolar electric fields of triangular waveform with a total time period of 60 s, with an effective frequency of ≈0.02 Hz. Each sample was electrically poled

using four successive electric field cycles of increasing magnitudes of ±1.0 kV mm$^{-1}$, ±1.5 kV mm$^{-1}$, ±2.0 kV mm$^{-1}$, and ±2.5 kV mm$^{-1}$. During every electric field application, the high-energy XRD patterns were recorded continuously in increments of 1 s exposure time. To investigate the domain wall motion at weak electric fields, in situ XRD measurements were also conducted at electric field strength of 0.2 kV mm$^{-1}$, which is below the macroscopic coercive field strength (approximately 0.5 kV mm$^{-1}$) of polycrystalline $BaTiO_3$ ceramics. The subcoercive in situ X-ray measurements were conducted on the electrically poled (after applying ± 2.5 kV mm$^{-1}$ field) $BaTiO_3$ samples using an electric field of bipolar square wave form (±0.2 kV mm$^{-1}$) at a frequency of 0.33 Hz. For each of the diffraction measurements, a large, representative volume fraction of a polycrystalline specimen was irradiated and XRD patterns were measured at all angles relative to the applied electric field (Figure S3, Supporting Information).

## Supporting Information

Supporting Information is available from the Wiley Online Library or from the author.

## Acknowledgements

This work was partially supported by the U.S. Department of the Army under contract number W911NF-09-1-0435, the U.S. National Science Foundation under award number DMR-0746902, and the Florida Cluster for Advanced Smart Sensor Technologies (FCASST) under "New Florida 2010". Use of the Advanced Photon Source was supported by the U. S. Department of Energy, Office of Science, Office of Basic Energy Sciences, under Contract No. DE-AC02-06CH11357. The authors gratefully acknowledge the help of Dr. Yang Ren and Dr. Guy Jennings at beamline 11-ID-C at the Advanced Photon Source and Prof. Ghatu Subhash for access to the SPS facilities. Also the authors acknowledge Dr. Shruti Banavara Seshadri and Dr. Goknur Tutunchu for help with in situ X-ray measurements and for helpful discussion.

Received: June 5, 2013
Revised: July 16, 2013
Published online: September 3, 2013

[1] J. Junquera, P. Ghosez, *Nat. Mater.* **2003**, *422*, 506.
[2] D. D. Dillon, G. B. Stephenson, S. K. Streiffer, J. A. Eastman1, O. Auciello, P. H. Fuoss, C. Thompson, *Science*, **2004**, *304*, 1650.
[3] Z. Zhao, V. Buscaglia, M. Viviani, M. T. Buscaglia, L. Mitoseriu, A. Testino, M. Nygren, M. Johnsson, P. Nanni, *Phys. Rev. B*, **2004**, *70*, 024107.
[4] M. T. Buscaglia, *Phys Rev B.* **2006**, *73*, 064114.
[5] H. T. Martirenat, J. C. Burfoot, *J. Phys. C: Solid State Phys.* **1974**, *7*, 3182.
[6] P. Zheng, J. L. Zhang, Y. Q. Tan, C. L. Wang, *Acta Mater.* **2012**, *60*, 5022.
[7] W. R. Buessem, L. E. Cross, A. K. Goswami, *J. Am. Ceram. Soc.* **1966**, *49*, 33.
[8] W. R. Buessem, L. E. Cross, A. K. Goswami, *J. Am. Ceram. Soc.* **1966**, *49*, 36.
[9] G. Arlt, D. Hennings, G. de With, *J. Appl. Phys.* **1985**, *58*, 1619.
[10] T. Hoshina, K. Takizawa, J. Li, T. Kasama, H. Kakemoto, T. Tsurumi, *Jpn. J. Appl. Phys.* **2008**, *47*, 7607.
[11] T. Hoshina, Y. Kigoshi, S. Hatta, H. Takeda, T. Tsurumi, *Jpn. J. Appl. Phys.* **2009**, *48*, 09KC01.
[12] W. Cao, C. A. Randall, *J. Phys. Chem. Solids* **1996**, *57*, 1499.
[13] V. Buscaglia, M. T. Buscaglia, M. Viviani, L. Mitoseriu, P. Nanni, V. Trefiletti, P. Piaggio, I. Gregora, T. Ostapchuk, J. Pokorný, J. Petzelt, *J. Eur. Ceram. Soc.* **2006**, *26*, 2889.
[14] V. A. Polotai, V. A. Ragulya, C. A. Randall, *Ferroelectrics* **2003**, *288*, 93.
[15] I. Fujii, M. Ugorek, S. Trolier-McKinstry, *J. Appl. Phys.* **2010**, *107*, 104116.
[16] K. Kinoshita, A. Yamaji, *J. Appl. Phys.* **1976**, *47*, 371.
[17] A. J. Bell, Grain size effects in barium titanate – revisited, *Proceedings of the 9th IEEE ISAF meeting*, IEEE, New York **1994**, 14.
[18] T. Hoshina, Y. Kigoshia, S. Hatta, T. Teranishi, H. Takeda, T. Tsurumi, *Ferroelectrics* **2010**, *402*, 29.
[19] G. Arlt, G. H. Peusens, *Ferroelectrics* **1983**, *48*, 213.
[20] C. Miclea, C. Tănăsoiu, I. Spânulescu, C. F. Miclea, A. Gheorghiu, L. Aamrandel, M. Cioangher, C. T. Miclea, *Romanian J. Info. Sci. Technol.* **2007**, *10*, 335.
[21] H. Takahashi, Y. Numamoto, J. Tani, S. Tsurekawa, *J. J. Appl. Phys.* **2006**, *45*, 7405.
[22] A. J. Bell, A. J. Moulson, L. E. Cross, *Ferroelectrics* **1984**, *54*, 147.
[23] E. C. Subbarao, M. C. McQuarrie, W. R. Buessem, *J. Appl. Phys.* **1957**, *28*, 1194.
[24] M. J. Hoffmann, M. Hammer, A. Endriss, D. C. Lupascu, *Acta Mater.* **2001**, *49*, 1301.
[25] D. A. Hall, A. Steuwer, B. Cherdhirunkorn, T. Mori, P. J. Withers, *J. Appl. Phys.* **2004**, *96*, 4245.
[26] J. L. Jones, E. B. Slamovich, K. J. Bowman, *J. Appl. Phys.* **2005**, *97*, 034113.
[27] H. Kungl, R. Theissmann, M. Knapp, C. Baehtz, H. Fuess, S. Wagner, T. Fett, M. J. Hoffmann, *Acta Mater.* **2007**, *55*, 1849.
[28] J. L. Jones, A. Pramanick, J. E. Daniels, *Appl. Phys. Lett.* **2008**, *93*, 152904.
[29] J. E. Daniels, W. Jo, J. Rödel, V. Honkimäi, J. L. Jones, *Acta Mater.* **2010**, *58*, 2103.
[30] A. Pramanick, D. Damjanovic, J. E. Daniels, J. C. Nino, J. L. Jones, *J. Am. Ceram. Soc.* **2011**, *94*, 293.
[31] J. L. Jones, E. Aksel, G. Tutuncu, T.-M. Usher, J. Chen, X. Xing, A. J. Studer, *Phys. Rev. B* **2012**, *86*, 024104.
[32] D. Ghosh, H. Han, J. C. Nino, G. Subhash, J. L. Jones, *J. Am. Ceram. Soc.* **2012**, *95*, 2504.
[33] S. Yoon, J. Dornseiffer, Y. Xiong, D. Grüner, Z. Shen, S. Iwaya, C. Pithan, R. Waser, *J. Eur. Ceram. Soc.* **2011**, *31*, 1723.
[34] G. Arlt, *Ferroelectrics* **1987**, *76*, 451.
[35] M. H. Frey, D. A. Payne, *Phys. Rev. B* **1996**, *54*, 3158.
[36] S. Wada, K. Yako, H. Kakemoto, T. Tsurumi, T. Kiguchi, *J. Appl. Phys.* **2005**, *98*, 014109.
[37] G. Arlt, N. A. Pertsev, *J. Appl. Phys.* **1991**, *70*, 2283.
[38] N. A. Pertsev, G. Arlt, *J. Appl. Phys.* **1993**, *74*, 4105.
[39] M. Demartin, D. Damjanovic, *Appl. Phys. Lett.* **1996**, *68*, 3046.
[40] G. Arlt, *J. Mater. Sci.* **1990**, *25*, 2655.
[41] A. E. Jacobs, *Phys. Rev. B* **1985**, *31*, 5984.
[42] J. E. Daniels, J. L. Jones, T. R. Finlayson, *J. Phys. D: Appl. Phys.* **2006**, *39*, 5294.
[43] F.-S. Yen, H.-I. Hsiang, Y.-H. Chang, *J. J. Appl. Phys.* **1995**, *34*, 6149.
[44] T. C. Huang, M. T. Wang, H. S. Sheu, W. F. Hsieh, *J. Phys.: Condens. Matter.* **2007**, *19*, 476212.
[45] G. Tutuncu, D. Damjanovic, J. Chen, J. L. Jones, *Phys. Rev. Letts.* **2012**, *108*, 177601.
[46] W. J. Merz, *Phys. Rev.* **1953**, *91*, 513.
[47] D. Meyerhofer, *Phys. Rev.* **1958**, *112*, 413.
[48] G. Picht, H. Kungl, M. Bäurer, M. J. Hoffmann, *Funct. Mater. Letts.* **2010**, *3*, 59.
[49] H. Cao, C. P. Devreugd, W. Ge, J. Li, D. Viehland, H. Luo, X. Zhao, *Appl. Phys. Lett.* **2009**, *94*, 032901.

[50] Y. Yoshimura, A. Kojimab, N. Tokunaga, K. Tozaki, T. Koganezawa, *Phys. Letts. A* **2006**, *353*, 250.
[51] A. Pramanick, D. Damjanovic, J. C. Nino, J. L. Jones, *J. Am. Ceram. Soc.* **2009**, *92*, 2291.
[52] A. Pramanick, J. Daniels, J. L. Jones, *J. Am. Ceram. Soc.* **2009**, *92*, 2300.
[53] J. L. Jones, J. E. Daniels, A. J. Studer, M. Hoffman, *Appl. Phys. Lett.* **2006**, *89*, 092901.
[54] L. E. Cross, *Ferroelectric ceramics: tailoring properties for specific applications, Ferroelectric Ceramics*, (Ed. N. Setter, E. L. Colla), Birkhäuser, Basel **1993**.
[55] D. Damjanovic, *Rep. Prog. Phys.* **1998**, *61*, 1267.
[56] Q. M. Zhang, W. Y. Pan, S.-J. Jang, L. E. Cross, *J. Appl. Phys.* **1988**, *64*, 6445.
[57] Q. M. Zhang, H. Wang, N. Kim, L. E. Cross, *J. Appl. Phys.* **1994**, *75*, 454.
[58] H. Hagemann, *J. Phys. C: Solid State Phys.* **1978**, *11*, 3333.
[59] D. Damjanovic, *J. Appl. Phys.* **1997**, *82*, 1788.
[60] D. Damjanovic, M. Demartin, *J. Phys: Condens Matter* **1997**, *9*, 4943.
[61] E. I. Bondarenko, Y. Y. Topolov, A. V. Turik, *Ferroelectr. Letts. Sec.* **1991**, *13*, 13.